Head-to-Head Comparison of ^{11}C-PiB and ^{18}F-AZD4694 (NAV4694) for β-Amyloid Imaging in Aging and Dementia

Christopher C. Rowe[1,2], Svetlana Pejoska[1], Rachel S. Mulligan[1], Gareth Jones[1], J. Gordon Chan[1], Samuel Svensson[3], Zsolt Cselényi[3], Colin L. Masters[4], and Victor L. Villemagne[1,2,4]

[1]Department of Nuclear Medicine and Centre for PET, Austin Health, Heidelberg, Victoria, Australia; [2]Department of Medicine, University of Melbourne, Parkville, Victoria, Australia; [3]AstraZeneca R&D, Södertälje, Sweden; and [4]The Mental Health Research Institute, University of Melbourne, Parkville, Victoria, Australia

^{11}C-Pittsburgh compound-B (^{11}C-PiB) is the benchmark radiotracer for imaging of β-amyloid (Aβ) plaque in Alzheimer disease (AD). ^{18}F-labeled Aβ tracers subsequently developed for clinical use show higher nonspecific white matter binding and, in some cases, lower cortical binding in AD that could lead to less accurate interpretation of scans. We compared the cortical and white matter binding of a new ^{18}F-labeled Aβ tracer, ^{18}F-AZD4694 (recently renamed NAV4694), with ^{11}C-PiB in the same subjects. **Methods:** Forty-five participants underwent PET imaging with ^{11}C-PiB and ^{18}F-AZD4694 (25 healthy elderly controls [HCs], 10 subjects with mild cognitive impairment, 7 subjects with probable AD, and 3 subjects with probable frontotemporal dementia). Images were coregistered so that region-of-interest placement was identical on both scans, and standardized uptake value ratios (SUVRs) using the cerebellar cortex as a reference region were calculated between 40 and 70 min after injection for both tracers. **Results:** ^{18}F-AZD4694 showed reversible binding kinetics similar to ^{11}C-PiB, reaching an apparent steady state at 50 min after injection. Both radiotracers showed a similar dynamic range of neocortical SUVR (1.1–3.3 and 1.0–3.2 SUVR for ^{11}C-PiB and ^{18}F-AZD4694, respectively) and identical low nonspecific white matter binding, with frontal cortex–to–white matter ratios of 0.7 ± 0.2 and 1.3 ± 0.2 for both radiotracers in HCs and AD subjects, respectively. There was an excellent linear correlation between ^{11}C-PiB and ^{18}F-AZD4694 neocortical SUVR (slope of 0.95, $r = 0.99$, $P < 0.0001$). **Conclusion:** ^{18}F-AZD4694 displays imaging characteristics nearly identical to those of ^{11}C-PiB. The low white matter and high cortical binding in AD indicate that this tracer is well suited to both clinical and research use.

Key Words: Alzheimer's disease; amyloid imaging; Aβ; positron emission tomography

Imaging of β-amyloid (Aβ) in vivo with PET provides an important new tool for the evaluation of the causes, diagnosis, and future treatment of dementias, where Aβ may play a role (*1*). Studies with ^{11}C-Pittsburgh compound-B (^{11}C-PiB), the first and most widely studied PET Aβ ligand, indicate that Aβ imaging may allow the earlier diagnosis of Alzheimer disease (AD) (*2,3*) and better differential diagnosis of dementia (*2,4*). ^{11}C-PiB studies show robust cortical binding in almost all AD subjects (*2,3*) and correlate well with a reduction in cerebral spinal fluid Aβ$_{42}$ (*5*) and AD histopathology (*6–8*). Increased ^{11}C-PiB binding has shown high predictive value for progression from mild cognitive impairment (MCI) to AD (*9,10*).

On the basis of recent advances in neuroimaging and cerebral spinal fluid analysis, the research criteria for the diagnosis of probable AD have been revised to allow for earlier diagnosis and therapeutic intervention (*11*). Thus, as the criteria for the diagnosis of AD evolve, Aβ imaging is likely to have an increasingly important role in clinical practice provided it is accessible and affordable and the scans can be read in a consistent and reliable manner when used beyond academic centers of excellence (*12*).

Unfortunately, the 20-min radioactive decay half-life of ^{11}C limits the use of ^{11}C-PiB to centers with an on-site cyclotron and ^{11}C radiochemistry expertise, making the access to ^{11}C-PiB PET restricted and with costs prohibitive for routine clinical use (*13*). To overcome these limitations, several tracers labeled with ^{18}F (half-life, 110 min)—which permits the centralized production and regional distribution, as currently practiced worldwide in the supply of ^{18}F-FDG for clinical use—were synthesized and tested (*14–18*). Florbetapir, florbetaben, and flutemetamol have completed phase III clinical trials, and florbetapir has been approved by the Food and Drug Administration for use in humans to detect the presence of amyloid plaques (*18–21*). However, these ^{18}F-labeled amyloid tracers have greater nonspecific white matter binding than ^{11}C-PiB and some have lower cortical binding in AD patients. These characteristics may make visual interpretation of scans more challenging, particularly for the detection of low levels of

cortical amyloid plaque, and increase the level of training and expertise required for accurate and consistent visual interpretation of scans in clinical practice.

A preliminary study with a recently developed ^{18}F-labeled amyloid tracer that has a close structural resemblance to ^{11}C-PiB, ^{18}F-AZD4694 (recently renamed NAV4694) (Fig. 1) (17), showed a robust separation between AD patients and healthy age-matched controls (HCs) and less white matter binding than reported with other ^{18}F-labeled amyloid tracers. To further characterize ^{18}F-AZD4694, the present study compared the cortical and white matter binding of ^{11}C-PiB and ^{18}F-AZD4694 in the same subjects.

MATERIALS AND METHODS

Study Participants

The study was approved by the Austin Health Human Research Ethics Committee. Written informed consent was obtained from all subjects before participation and also from the next of kin or caregiver for the subjects with dementia. Participants were clinically classified by consensus between a neurologist and a neuropsychologist. The study was prospective and included 25 HCs, 10 subjects meeting criteria for mild cognitive impairment (MCI) (22), 10 subjects with dementia, 7 subjects meeting the criteria of the National Institute of Neurological Disorders and Stroke and the Alzheimer's Disease and Related Disorders Association for probable AD (23), and 3 subjects meeting criteria for frontotemporal dementia (FTD) (24). Subjects were recruited from the Austin Health Memory Disorders Clinic and affiliated dementia specialist clinics and by advertising.

All subjects were older than 60 y, spoke fluent English, and had completed at least 7 y of education. No subjects had a history of or physical or imaging findings of other neurologic/psychiatric illness, current or recent drug or alcohol abuse/dependence, or any significant other disease or unstable medical condition. Total radiation exposure from this study fell within the Australian guidelines for research radiation exposure for subjects older than 60 y.

More than half of the participants (56%) underwent the ^{11}C-PiB and ^{18}F-AZD4694 PET studies on the same day, with ^{18}F-AZD4694 administered 50 min after the ^{11}C-PiB study acquisition was fin-ished. The rest of the participants underwent the ^{11}C-PiB and ^{18}F-AZD4694 PET studies on separate occasions, with a median interval of 14 (±27) days (range, 1–93 d).

Participants were administered the Mini-Mental State Examination, were given a Clinical Dementia Rating score, and underwent a battery of neuropsychologic tests to ensure that they fulfilled diagnostic criteria for AD, MCI, or normality. A composite episodic memory score was calculated by taking the average of the z scores (generated using 65 low ^{11}C-PiB HC with normal MR imaging findings as the reference) for the Rey Complex Figure Test (30 min) long delay and California Verbal Learning Test–Second Edition long delay, as previously described (25). A composite nonmemory cognition score was calculated by taking the average of the z scores for the Boston Naming Test, letter fluency, category fluency, Digit Span forward and backward, Digit Symbol-Coding, and Rey Complex Figure Test copy.

Image Acquisition

MR imaging consisted of a 3-dimensional T1-weighted magnetization-prepared rapid gradient-echo scan used for screening and coregistration with the PET images.

PiB and AZD4694 were radiolabeled at the Centre for PET, Austin Health, as previously described (2,17). Briefly, PiB was produced using the 1-step ^{11}C-methyl triflate approach. The average radiochemical yield was 30% after a synthesis time of 45 min, with a radiochemical purity of greater than 98% and a specific activity of 30 ± 7.5 GBq/μmol. AZD4694 was produced by radio-fluorination of the corresponding N-Boc–protected nitro precursor, followed by acidic deprotection with hydrochloric acid. Average radiochemical yield was 16% after a synthesis time of 65 min, with a radiochemical purity of greater than 98% and a specific activity of 555 ± 230 GBq/μmol. PET scans were acquired on a 3-dimensional Phillips Allegro scanner at the Austin Health Centre for PET. A transmission scan using a rotating ^{137}Cs source was acquired for attenuation correction immediately before the emission scan. Participants underwent dynamic PET scans from 0 to 70 min after the injection 200 MBq of ^{18}F-AZD4694 and static scans at 40–70 min after the injection of 370 MBq of ^{11}C-PiB. Images were reconstructed using a 3-dimensional row-action maximum-likelihood algorithm.

Visual Inspection

Deidentified images were read separately by 3 independent readers masked to clinical diagnosis. Images were graded as no cortical binding, low cortical binding, or high cortical binding. The readers had variable experience with ^{11}C-PiB image interpretation, but none had prior experience with ^{18}F-AZD4964 PET. Transverse, sagittal, and coronal views were available for examination.

Image Analysis

Each individual's PET and MR images were coregistered using SPM5 (26). Regions of interest (ROIs) were then drawn on the individual MR images and transferred to the coregistered PET images (Supplemental Fig. 1; supplemental materials are available online only at http://jnm.snmjournals.org). Mean radioactivity values were obtained from ROIs for cortical, subcortical, and cerebellar regions. White matter ROIs were placed at the centrum semiovale, and the cerebellar regions were placed over the cerebellar cortex with care taken to avoid white matter. No correction for partial volume was applied to the PET data.

Standardized uptake values (SUVs)—defined as the decay-corrected brain radioactivity concentration, normalized for injected dose and body weight—were calculated for all regions. These
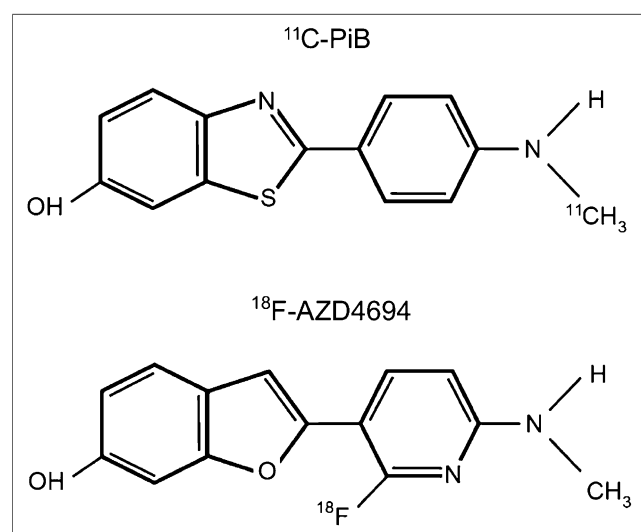

FIGURE 1. Chemical structure of ^{11}C-PiB and ^{18}F-AZD4694.

values were then used to derive the SUV ratio (SUVR) referenced to the cerebellar cortex (Supplemental Appendix 1), a region relatively unaffected by dense Aβ plaques in sporadic AD, for both ^{11}C-PiB and ^{18}F-AZD4694. Global Aβ burden was expressed as the average SUVR of the mean for the following cortical ROIs: frontal (consisting of dorsolateral prefrontal, ventrolateral prefrontal, and orbitofrontal regions), superior parietal, lateral temporal, lateral occipital, and anterior/posterior cingulate and precuneus. Distribution volume ratios (DVRs) for ^{18}F-AZD4694 were determined through graphical analysis of the 70-min time–activity curves (Supplemental Appendix 1) (27). The global DVR was calculated with the same regions used for the global SUVR.

As previously described (9) and to identify a SUVR cutoff, a hierarchical cluster analysis was performed on the 25 HC participants that yielded a threshold for high or low global SUVR of 1.5 for both ^{11}C-PiB and ^{18}F-AZD4694.

Statistical Evaluation

The normality of distribution was analyzed using the Shapiro–Wilk test and visual inspection of variable histograms. Statistical evaluations between radiotracers were performed using a paired Student t test, and comparisons to establish differences between group means were performed with ANOVA. Effect size was measured with Cohen d (Supplemental Appendix 1). Categoric differences were evaluated using a Fisher exact test. Pearson product–moment correlation analyses were conducted between ^{11}C-PiB and ^{18}F-AZD4694 SUVR. Data are presented as mean ± SD unless otherwise stated.

RESULTS

Forty-five participants were evaluated with both radiotracers, and their demographics are detailed in Table 1. No serious adverse events related to the study drugs were observed or reported by any participants as a result of the ^{11}C-PiB or ^{18}F-AZD4694 scans, and no concerns were raised by the participants or their relatives.

Brain radioactivity peaked between 3 and 6 min after injection of ^{18}F-AZD4694. The binding appeared to be reversible, with rapid washout from all areas in controls other than white matter, clearing fastest from the cerebellar cortex (Fig. 2) in keeping with a previous report (17). The clearance rate and the SUV measurements in the cerebellar cortex showed no difference between subject groups, consistent with the absence of significant Aβ in this region. In AD patients, cortical binding exceeded white matter binding at all time points (Fig. 2). The cortical–to–cerebellar gray matter ratio (SUVR) reached an apparent steady state approximately 50 min after injection in HCs and AD subjects, as previously reported (17). Given the similar brain kinetics between ^{11}C-PiB and ^{18}F-AZD4694, the same period of 40–70 min after injection was selected for the comparison.

There was an excellent linear correlation between DVR calculated from the 70-min dynamic scan and the SUVR calculated from the summed 40- to 70-min data of the ^{18}F-AZD4694 scans ($r = 0.95$, $P < 0.0001$, where ^{18}F-AZD4694 SUVR = ^{18}F-AZD4694 DVR × 1.85 − 0.66).

On visual inspection, the summed 40- to 70-min images of all AD subjects showed extensive cortical ^{11}C-PiB and ^{18}F-AZD4694 binding that was greater in the frontal and posterior cingulate and precuneus cortex and slightly less in the lateral temporal and parietal cortex. There was relative sparing of the primary sensorimotor cortex, with no appreciable specific binding in the cerebellar cortex. No cortical binding was observed in the 3 FTD patients. Six of the 10 (60%) MCI subjects presented with ^{11}C-PiB and ^{18}F-AZD4694 binding similar to that observed in the AD group. Twenty-one of the 25 HCs presented no cortical or subcortical gray matter ^{11}C-PiB or ^{18}F-AZD4694 binding, and their scans were clearly distinguishable from subjects with AD. However, 4 (16%) HCs were visually classified as having cortical ^{11}C-PiB binding, and cortical ^{18}F-AZD4694 binding was also observed in the same 4 HCs.

The ^{11}C-PiB and ^{18}F-AZD4694 images were virtually indistinguishable by visual inspection (Fig. 3). Similar white matter binding was observed with both radiotracers. When quantified, there were no significant differences in white matter binding for each tracer in both HCs and AD subjects, with frontal cortex–to–white matter ratios of 0.72 ± 0.16 and 1.36 ± 0.22, respectively, for ^{11}C-PiB and 0.71 ± 0.16 and 1.33 ± 0.22, respectively, for ^{18}F-AZD4694.

TABLE 1
Cohort Demographics

Demographic	HC ($n = 25$)	MCI ($n = 10$)	FTD ($n = 3$)	AD ($n = 7$)
Age	74.0 ± 7.9	74.8 ± 9.2	68.1 ± 4.6	73.1 ± 10.9
Sex				
Male	8	7	2	5
Female	17	3	1	2
Years of education	14.3 ± 3.7	13.0 ± 4.5	12.0 ± 3.5	11.3 ± 3.7
Mini-Mental State Examination	28.8 ± 0.9	26.6 ± 2.6*	26.7 ± 1.2	23.7 ± 2.4*
Clinical Dementia Rating	0.0	0.45 ± 0.16*	0.83 ± 0.29*	0.71 ± 0.27*
Episodic memory	−0.01 ± 0.8	−2.7 ± 0.7*	−3.7 ± 0.4*	−3.1 ± 0.6*
Nonmemory	0.1 ± 0.5	−1.2 ± 0.9*	−2.6 ± 0.4*	−2.3 ± 1.3*
ApoE ε4 (%)	30	70*	33	57*

*Significantly different from HC ($P < 0.05$).
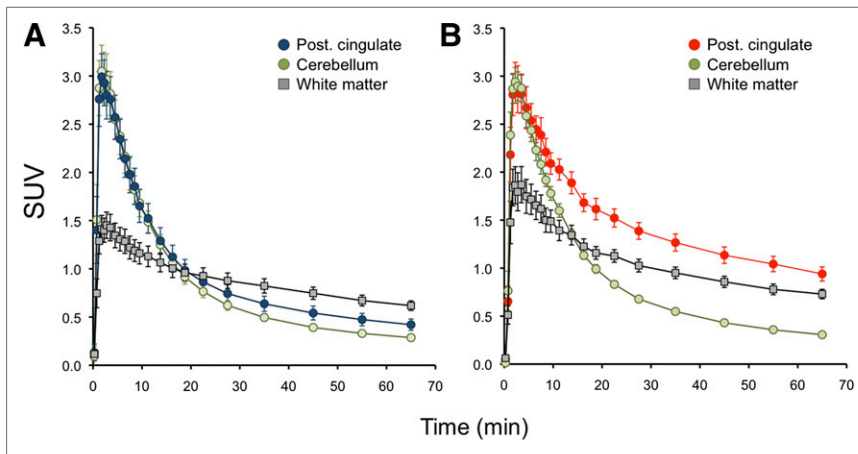
FIGURE 2. Time–activity curves for ^{18}F-AZD4694 in HCs and AD subjects. Mean time–activity curves from 25 HCs (A) and 7 AD patients (B). In AD group, at all time points, cortical binding exceeds white matter binding.

Figure 4 shows the global cortical SUVR for ^{11}C-PiB and ^{18}F-AZD4694. Global ^{11}C-PiB SUVRs were 1.31 ± 0.25 in HCs, 2.00 ± 0.70 in MCI subjects, 2.45 ± 0.50 in AD subjects, and 1.26 ± 0.14 in FTD subjects. Similar values were obtained with ^{18}F-AZD4694 for the same groups, with SUVRs of 1.27 ± 0.22 in HCs, 1.97 ± 0.66 in MCI subjects, 2.41 ± 0.45 in AD subjects, and 1.26 ± 0.11 in FTD subjects. Despite the similar SUVRs, when HCs were compared with AD subjects, ^{18}F-AZD4694 yielded a slightly higher effect size ($d = 2.6$ and 2.9 for ^{11}C-PiB and ^{18}F-AZD4694, respectively). When the cutoff SUVR of 1.50 was applied, 4 (16%) HCs were considered to have high Aβ burden with ^{11}C-PiB, whereas only 3 (12%) HCs were considered to have high Aβ burden with ^{18}F-AZD4694. The discrepant HC had an SUVR of 1.54 for ^{11}C-PiB and an SUVR of 1.49 for ^{18}F-AZD4694. All gray matter regions in the AD group were significantly higher than those in the HC group. Table 2 lists the global and regional SUVRs for both radiotracers, along with the respective effect size for each region in the HC and AD groups. Percentage differences in cortical SUVRs between ^{11}C-PiB and ^{18}F-AZD4694 (1.5% and 1.2% for HC and AD groups, respectively) were well below our 3.5% test–retest reproducibility for ^{11}C-PiB (9).

The Mini-Mental State Examination scores correlated with ^{11}C-PiB global SUVRs ($r = -0.66$, $P < 0.0001$) and ^{18}F-AZD4694 global SUVRs ($r = -0.69$, $P < 0.0001$) when all subjects were pooled together. Similarly, when pooled together, global SUVRs also correlated with episodic memory ($r = -0.50$, $P = 0.0008$ and $r = -0.53$, $P = 0.0004$ for ^{11}C-PiB and ^{18}F-AZD4694, respectively) and nonmemory scores ($r = -0.57$, $P < 0.0001$ and $r = -0.61$, $P < 0.0001$ for ^{11}C-PiB and ^{18}F-AZD4694, respectively). However, when cohorts were analyzed separately, there was no significant correlation in any group, with the exception of global ^{18}F-AZD4694 SUVR and episodic memory scores in HCs ($r = -0.44$, $P = 0.039$). No such correlation was found for ^{11}C-PiB ($r = -0.33$, $P = 0.12$).

There was a high correlation between ^{11}C-PiB and ^{18}F-AZD4694 global SUVRs ($r = 0.99$, $P < 0.0001$) as de-

scribed by the following equation: ^{18}F-AZD4694 global SUVR = (^{11}C-PiB global SUVR × 0.95) + 0.05 (Fig. 5). The high correlation between ^{11}C-PiB and ^{18}F-AZD4694 SUVR remained when the HC, MCI, and AD groups were examined separately ($r = 0.96$, $P < 0.0001$; $r = 0.99$, $P < 0.0001$; and $r = 0.93$, $P = 0.0021$, respectively). Regional cortical, subcortical, and white matter area SUVRs for ^{11}C-PiB and ^{18}F-AZD4694 were also highly correlated (Table 3).

DISCUSSION

Aβ imaging is a tool that has opened up new possibilities for the early detection, intervention, and prevention of
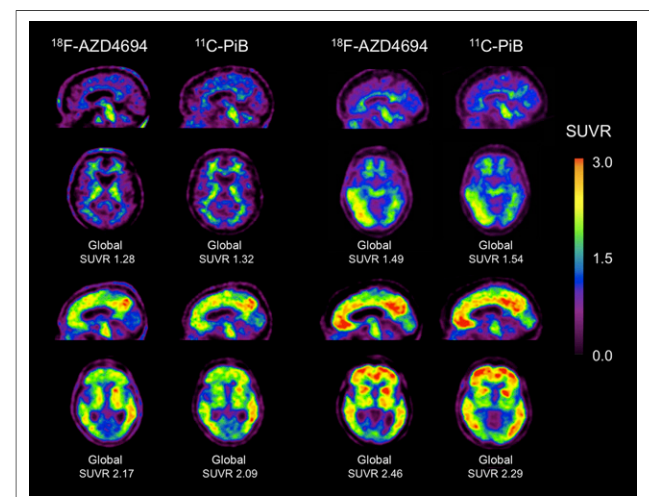
FIGURE 3. ^{18}F-AZD4694 and ^{11}C-PiB PET imaging in 4 subjects representative of range of tracer binding. Four examples of sagittal and transaxial ^{18}F-AZD4694 images adjacent to same-slice ^{11}C-PiB images in same subject. Top 2 subjects were HCs, and bottom 2 both had clinical diagnosis of AD. ^{18}F-AZD4694 and ^{11}C-PiB images were acquired with same acquisition time frame, processed in the same manner, and are shown scaled to same SUVR maximum, illustrating near-identical appearance and dynamic range of SUVRs of ^{18}F-AZD4694 to ^{11}C-PiB. Low-level, predominantly right occipitotemporal cortical binding is equally well detected in asymptomatic, elderly subject (top right).

FIGURE 4. Global Aβ burden with ^{11}C-PiB and ^{18}F-AZD4694. Box plots of global Aβ burden in same HC, MCI, FTD, and AD participants assessed with ^{11}C-PiB (A) or ^{18}F-AZD4694 (B). Dotted line denotes 1.5 threshold between high and low radiotracer binding. *Significantly different from HC ($P < 0.05$).
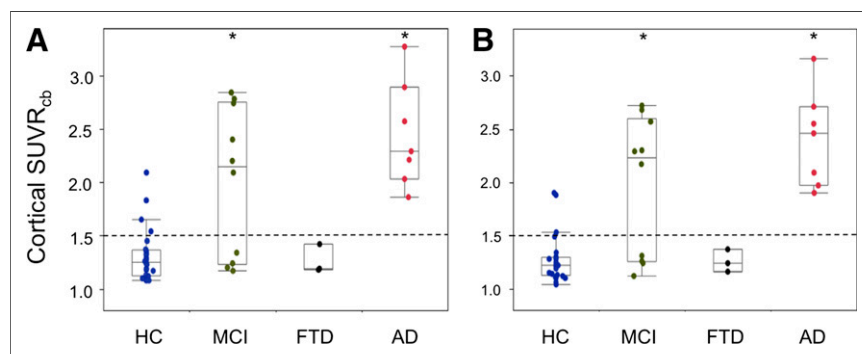
dementia due to AD. In addition to an emerging role in dementia diagnosis in clinical practice, Aβ imaging is likely to play a critical role in the development of anti-amyloid therapies, by improving subject selection at early phases of the disease and monitoring treatment response.

To our knowledge, this is the first report directly comparing ^{11}C-PiB and ^{18}F-AZD4694 in the same subjects, comprising the following 4 different clinical groups: HCs, MCI patients, FTD patients, and AD patients. As expected, the AD group showed higher Aβ burden than did HCs, as measured by both ^{11}C-PiB and ^{18}F-AZD4694 binding.

^{18}F-AZD4694 provided a robust separation of AD patients from HCs. This separation was achieved either with visual image inspection or with a simple quantitative measure, the global SUVR (i.e., the ratio of cortical–to–cerebellar gray matter binding), derived from a scan with an acquisition length suitable for clinical imaging. It appears likely

that scan duration can be reduced without compromising sensitivity or image quality, but this requires further investigation and validation. Furthermore, compared with ^{11}C-PiB, both the use of ^{18}F-labeled amyloid tracers and the decay half-life of ^{18}F make centralized production with distribution to multiple PET sites possible, thereby improving access to Aβ imaging.

Visually, 16% of HCs were deemed positive for Aβ as assessed by both ^{11}C-PiB and ^{18}F-AZD4694, presenting an almost identical regional pattern of cortical binding. As in numerous reports, this finding suggests that Aβ deposition is an early feature of the disease preceding cognitive impairment (*2,28–31*). The prevalence of ^{18}F-AZD4694–positive scan findings reported here is in accord with previous reports using ^{11}C-PiB (*2,28,29*) and with postmortem studies that have documented moderate numbers of Aβ plaques in the cerebral cortex of about a quarter of nondemented persons older than 75 y (*30,31*).

TABLE 2
Comparison of ^{18}F-AZD4694 and ^{11}C-PiB SUVRs and Effect Sizes (*d*) in HCs and AD Subjects

Region	^{18}F-AZD4694			^{11}C-PiB		
	HC	AD	*d* ^{18}F-AZD4694	HC	AD	*d* ^{11}C-PiB
Dorsolateral prefrontal	1.21 ± 0.22	2.28 ± 0.50*	2.8	1.24 ± 0.25	2.41 ± 0.73†	2.2
Ventrolateral prefrontal	1.29 ± 0.26	2.57 ± 0.58*	2.8	1.31 ± 0.29	2.62 ± 0.67*	2.6
Orbitofrontal	1.31 ± 0.27	2.48 ± 0.52*	2.8	1.32 ± 0.30	2.32 ± 0.39‡*	2.9
Gyrus rectus	1.34 ± 0.27	2.58 ± 0.55*	2.9	1.35 ± 0.28	2.47 ± 0.43‡	3.1
Anterior cingulate	1.21 ± 0.26	2.39 ± 0.59*	2.6	1.23 ± 0.31	2.42 ± 0.55*	2.6
Precuneus and posterior cingulate	1.28 ± 0.32	2.76 ± 0.43‡	4.0	1.31 ± 0.36	2.81 ± 0.46‡	3.6
Parietal	1.21 ± 0.29	2.27 ± 0.46‡	2.8	1.26 ± 0.32	2.38 ± 0.58*	2.4
Lateral occipital	1.38 ± 0.18	1.97 ± 0.42†	1.9	1.42 ± 0.22	2.06 ± 0.48†	1.7
Lateral temporal	1.31 ± 0.21	2.53 ± 0.49‡	3.2	1.35 ± 0.22	2.54 ± 0.51*	3.0
Mesial temporal	1.32 ± 0.14	1.72 ± 0.23*	2.1	1.28 ± 0.14	1.70 ± 0.34†	1.6
Caudate nuclei	1.42 ± 0.22	2.62 ± 0.34‡	4.2	1.39 ± 0.26	2.46 ± 0.30‡	3.8
Putamen	1.36 ± 0.17	2.18 ± 0.22‡	4.2	1.36 ± 0.20	2.14 ± 0.23‡	3.7
Thalamus	1.36 ± 0.17	1.75 ± 0.18*	2.3	1.28 ± 0.20	1.74 ± 0.22*	2.2
Pons	2.13 ± 0.16	2.31 ± 0.59	0.4	2.22 ± 0.22	2.35 ± 0.59	0.3
White matter	1.83 ± 0.21	2.08 ± 0.37	0.8	1.83 ± 0.21	2.13 ± 0.53	0.8
Neocortex†	1.28 ± 0.25	2.41 ± 0.50‡	2.9	1.30 ± 0.28	2.44 ± 0.55*	2.6

*Significantly different from HC ($P < 0.005$).
†Significantly different from HC ($P < 0.05$).
‡Significantly different from HC ($P < 0.0005$).
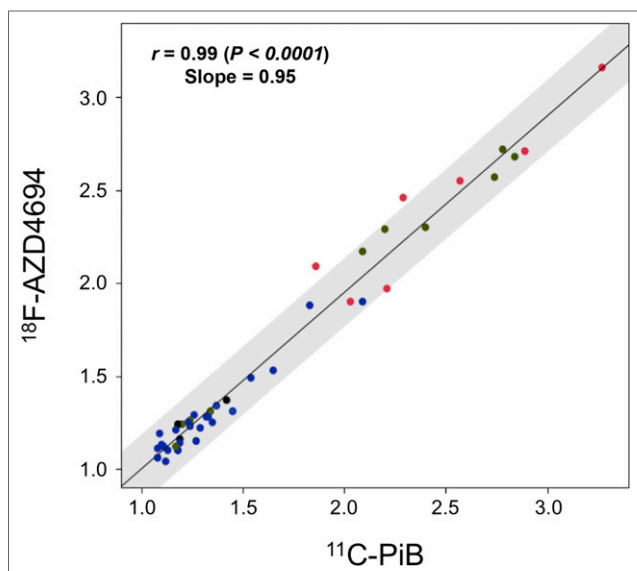
FIGURE 5. Same subject correlation of global SUVR for ^{11}C-PiB and ^{18}F-AZD4694. High correlation is observed between ^{11}C-PiB and ^{18}F-AZD4694 ($r = 0.99$; $P < 0.0001$). Slope of 0.95 indicates that spectrum of ^{18}F-AZD4694 value is almost identical to that for ^{11}C-PiB. Red dots are AD subjects ($n = 7$), black are FTD subjects ($n = 3$), green are MCI subjects ($n = 10$), and blue are HCs ($n = 25$).

The cortical distribution was almost identical for both tracers, displaying the same dynamic range of SUVRs, with mean global SUVR for AD being 87% greater than in HC with ^{11}C-PiB and 90% greater with ^{18}F-AZD4694. ^{18}F-AZD4694 also had a slightly higher effect size than ^{11}C-PiB (2.9 vs. 2.6, respectively).

The relatively low degree of nonspecific binding to white matter in ^{18}F-AZD4694 studies distinguishes this compound from the ^{18}F amyloid radiotracers that are currently in late-stage clinical trials or approved for clinical use (*2,15,16,18,32*). Similar cortical–to–white matter ratios were obtained for both ^{11}C-PiB and ^{18}F-AZD4694 in HCs and AD subjects, and the ratio in AD is substantially higher than those reported for other ^{18}F amyloid radiotracers (*2,15,16,18,32*).

Likewise, the slope of the linear correlation of ^{18}F-AZD4694 to ^{11}C-PiB of 0.95 is higher than those reported for florbetapir (with reported slopes ranging from 0.33 to 0.64) (*33,34*) and florbetaben (slope of 0.71) (*35*), and this translates to a wider dynamic range with greater percentage difference between the mean global SUVRs of HCs and AD cohorts and greater image contrast between HC and AD.

Given this low, nonspecific white matter binding and the high cortical binding in AD, visual reading of scans may be less challenging for ^{18}F-AZD4694 than for the other ^{18}F amyloid radiotracers. In AD, ^{18}F-AZD4694 PET images clearly show high radiotracer binding in extensive areas of gray matter well in excess of white matter binding. In contrast, other ^{18}F amyloid radiotracers show cortical binding frequently similar to, rather than greater than, the nonspecific white matter binding, leading to the recommen-

dation that the criteria for a positive florbetapir scan finding for cortical amyloid include loss of the gray–white matter demarcation in 2 or more areas of the brain (*14*). A direct comparison of ^{18}F-AZD4694 to other ^{18}F-labeled amyloid tracers is required to determine what impact this difference has on the accuracy of visual interpretation and ability to detect small changes in brain amyloid load over time or with treatment.

CONCLUSION

Our results demonstrate that ^{18}F-AZD4694 is highly correlated with ^{11}C-PiB and therefore should reliably detect Aβ deposition in the brain and be useful in the early and differential diagnosis of AD. ^{18}F-AZD4694 provides images that appear similar to those of ^{11}C-PiB, without the limitation of the short ^{11}C radioactive decay half-life that precludes the application of ^{11}C-PiB in clinical practice. The striking similarity with ^{11}C-PiB suggests that the results from longitudinal studies that are clarifying the relationship between Aβ accumulation and cognitive decline, and asserting the value of Aβ imaging as a predictor of cognitive decline and progression to clinical AD, can be directly translated to ^{18}F-AZD4694. The high cortical binding in AD and low nonspecific white matter binding also suggests that ^{18}F-AZD4694 images may be more easily and reliably read in clinical practice than other ^{18}F-labeled PET tracers for brain amyloid.

DISCLOSURE

TABLE 3
Regional Correlation Coefficients for ^{11}C-PiB and
^{18}F-AZD4694 SUVRs

Region	r	P
Dorsolateral prefrontal	0.95	<0.0001
Ventrolateral prefrontal	0.99	<0.0001
Orbitofrontal	0.95	<0.0001
Gyrus rectus	0.95	<0.0001
Anterior cingulate	0.98	<0.0001
Precuneus and posterior cingulate	0.99	<0.0001
Parietal	0.97	<0.0001
Lateral occipital	0.96	<0.0001
Lateral temporal	0.99	<0.0001
Mesial temporal	0.95	<0.0001
Caudate nuclei	0.98	<0.0001
Putamen	0.98	<0.0001
Thalamus	0.88	<0.0001
Pons	0.87	<0.0001
White matter	0.79	<0.0001
Global*	0.99	<0.0001

*Global comprises average SUVR for frontal, parietal, precuneus, cingulate, lateral occipital, and lateral temporal cortices.

ACKNOWLEDGMENTS

REFERENCES

1. Villemagne VL, Fodero-Tavoletti MT, Pike KE, Cappai R, Masters CL, Rowe CC. The ART of loss: Aβ imaging in the evaluation of Alzheimer's disease and other dementias. *Mol Neurobiol.* 2008;38:1–15.
2. Rowe CC, Ng S, Ackermann U, et al. Imaging beta-amyloid burden in aging and dementia. *Neurology.* 2007;68:1718–1725.
3. Klunk WE, Engler H, Nordberg A, et al. Imaging brain amyloid in Alzheimer's disease with Pittsburgh Compound-B. *Ann Neurol.* 2004;55:306–319.
4. Rabinovici GD, Furst AJ, O'Neil JP, et al. ^{11}C-PIB PET imaging in Alzheimer disease and frontotemporal lobar degeneration. *Neurology.* 2007;68:1205–1212.
5. Fagan AM, Mintun MA, Mach RH, et al. Inverse relation between in vivo amyloid imaging load and cerebrospinal fluid Abeta$_{42}$ in humans. *Ann Neurol.* 2006;59:512–519.
6. Bacskai BJ, Frosch MP, Freeman SH, et al. Molecular imaging with Pittsburgh Compound B confirmed at autopsy: a case report. *Arch Neurol.* 2007;64:431–434.
7. Leinonen V, Alafuzoff I, Aalto S, et al. Assessment of beta-amyloid in a frontal cortical brain biopsy specimen and by positron emission tomography with carbon 11-labeled Pittsburgh Compound B. *Arch Neurol.* 2008;65:1304–1309.
8. Ikonomovic MD, Klunk WE, Abrahamson EE, et al. Post-mortem correlates of in vivo PiB-PET amyloid imaging in a typical case of Alzheimer's disease. *Brain.* 2008;131:1630–1645.
9. Villemagne VL, Pike KE, Chetelat G, et al. Longitudinal assessment of Aβ and cognition in aging and Alzheimer disease. *Ann Neurol.* 2011;69:181–192.
10. Nordberg A, Carter SF, Rinne J, et al. A European multicentre PET study of fibrillar amyloid in Alzheimer's disease. *Eur J Nucl Med Mol Imaging.* 2013;40:104–114.
11. McKhann GM, Knopman DS, Chertkow H, et al. The diagnosis of dementia due to Alzheimer's disease: Recommendations from the National Institute on Aging-Alzheimer's Association workgroups on diagnostic guidelines for Alzheimer's disease. *Alzheimers Dement.* 2011;7:263–269.
12. Rowe CC, Villemagne VL. Brain amyloid imaging. *J Nucl Med.* 2011;52:1733–1740.
13. Villemagne VL, Rowe CC. Amyloid PET ligands for dementia. *PET Clin.* 2010;5:33–53.
14. Rowe CC, Ackerman U, Browne W, et al. Imaging of amyloid beta in Alzheimer's disease with ^{18}F-BAY94-9172, a novel PET tracer: proof of mechanism. *Lancet Neurol.* 2008;7:129–135.
15. Wong DF, Rosenberg PB, Zhou Y, et al. In vivo imaging of amyloid deposition in Alzheimer disease using the radioligand ^{18}F-AV-45 (flobetapir F 18). *J Nucl Med.* 2010;51:913–920.
16. Vandenberghe R, Van Laere K, Ivanoiu A, et al. ^{18}F-flutemetamol amyloid imaging in Alzheimer disease and mild cognitive impairment: a phase 2 trial. *Ann Neurol.* 2010;68:319–329.
17. Cselényi Z, Jonhagen ME, Forsberg A, et al. Clinical validation of ^{18}F-AZD4694, an amyloid-beta-specific PET radioligand. *J Nucl Med.* 2012;53:415–424.
18. Clark CM, Schneider JA, Bedell BJ, et al. Use of florbetapir-PET for imaging beta-amyloid pathology. *JAMA.* 2011;305:275–283.
19. Buckley C, Ikonomovic M, Smith A, et al. Flutemetamol F 18 injection PET images reflect brain beta-amyloid levels [abstract]. *Alzheimers Dement.* 2012;8(suppl):90.
20. Clark CM, Pontecorvo MJ, Beach TG, et al. Cerebral PET with florbetapir compared with neuropathology at autopsy for detection of neuritic amyloid-beta plaques: a prospective cohort study. *Lancet Neurol.* 2012;11:669–678.
21. Sabbagh M, Seibyl J, Akatsu H, et al. Multicentre phase 3 trial on florbetaben for beta-amyloid brain PET in Alzheimer's disease [abstract]. *Alzheimers Dement.* 2012;8(suppl):90.
22. Winblad B, Palmer K, Kivipelto M, et al. Mild cognitive impairment–beyond controversies, towards a consensus: report of the International Working Group on Mild Cognitive Impairment. *J Intern Med.* 2004;25:240–246.
23. McKhann G, Drachman D, Folstein M, Katzman R, Price D, Stadlan EM. Clinical diagnosis of Alzheimer's disease: report of the NINCDS-ADRDA Work Group under the auspices of Department of Health and Human Services Task Force on Alzheimer's Disease. *Neurology.* 1984;34:939–944.
24. McKhann GM, Albert MS, Grossman M, Miller B, Dickson D, Trojanowski JQ. Clinical and pathological diagnosis of frontotemporal dementia: report of the Work Group on Frontotemporal Dementia and Pick's Disease. *Arch Neurol.* 2001;58:1803–1809.
25. Pike KE, Savage G, Villemagne VL, et al. Beta-amyloid imaging and memory in non-demented individuals: evidence for preclinical Alzheimer's disease. *Brain.* 2007;130:2837–2844.
26. Good CD, Johnsrude IS, Ashburner J, Henson RN, Friston KJ, Frackowiak RS. A voxel-based morphometric study of ageing in 465 normal adult human brains. *Neuroimage.* 2001;14:21–36.
27. Logan J, Fowler JS, Volkow ND, Wang GJ, Ding YS, Alexoff DL. Distribution volume ratios without blood sampling from graphical analysis of PET data. *J Cereb Blood Flow Metab.* 1996;16:834–840.
28. Aizenstein HJ, Nebes RD, Saxton JA, et al. Frequent amyloid deposition without significant cognitive impairment among the elderly. *Arch Neurol.* 2008;65:1509–1517.
29. Villemagne VL, Pike KE, Darby D, et al. Aβ deposits in older non-demented individuals with cognitive decline are indicative of preclinical Alzheimer's disease. *Neuropsychologia.* 2008;46:1688–1697.
30. Bennett DA, Schneider JA, Arvanitakis Z, et al. Neuropathology of older persons without cognitive impairment from two community-based studies. *Neurology.* 2006;66:1837–1844.
31. Price JL, Morris JC. Tangles and plaques in nondemented aging and "preclinical" Alzheimer's disease. *Ann Neurol.* 1999;45:358–368.
32. Villemagne VL, Ong K, Mulligan RS, et al. Amyloid imaging with ^{18}F-florbetaben in Alzheimer disease and other dementias. *J Nucl Med.* 2011;52:1210–1217.
33. Wolk DA, Zhang Z, Boudhar S, Clark CM, Pontecorvo MJ, Arnold SE. Amyloid imaging in Alzheimer's disease: comparison of florbetapir and Pittsburgh compound-B positron emission tomography. *J Neurol Neurosurg Psychiatry.* 2012;83:923–926.
34. Landau SM, Breault C, Joshi AD, et al. Amyloid-β imaging with Pittsburgh Compound B and florbetapir: comparing radiotracers and quantification methods. *J Nucl Med.* 2013;54:70–77.
35. Villemagne VL, Mulligan RS, Pejoska S, et al. Comparison of ^{11}C-PiB and ^{18}F-florbetaben for Aβ imaging in ageing and Alzheimer's disease. *Eur J Nucl Med Mol Imaging.* 2012;39:983–989.